UCRL- 84854
PREPRINT

MASTER

STIMULATED RAMAN SCATTERING IN LARGE PLASMAS

Donald J. Phillion
David J. Banner

This paper was prepared for submittal
to the American Physical Society, Division
of Plasma Physics Meeting in San Diego, Calif.
November 10-14, 1980

November 6, 1980

Lawrence Livermore Laboratory

Stimulated Raman Scattering In Large Plasmas

D. W. Phillion and D. L. Banner

Abstract

Stimulated Raman scattering is of concern to laser fusion since it can create a hot electron environment which can increase the difficulty of achieving high final fuel densities. In earlier experiments with one micron laser light, the energy measured in Raman-scattered light has been insignificant. But these experiments were done with, at most, about 100 joules of laser energy. The Raman instability has a high threshold which also requires a large plasma to be irradiated with a large diameter spot. Only with a long interaction length can the Raman-scattered light wave convectively grow to a large amplitude, and only in recent long pulse, high energy experiments (4000 joules in 2 ns) at the Shiva laser facility have we observed as much as several percent of the laser light to be Raman-scattered.

We find that the Raman instability has a much lower intensity threshold for longer laser pulselength and larger laser spot size on a solid target. The spectrum of the Raman-scattered light has been measured from 1.48 to 2.17 μm with a liquid nitrogen cooled indium arsenide detector array. We find the Raman-scattering is occurring not only at quarter critical density, but also at much lower electron densities. The data suggest that Raman side-scatter may be occurring. We also report preliminary Raman light measurements for 5320Å (green light) solid target experiments. A strong polarization dependence was observed in the Raman light originating at low electron densities.

---

* Work performed under the auspices of the U. S. Department of Energy by the Lawrence Livermore Laboratory under Contract No. W-7405-ENG-48.

I Introduction

Laser fusion targets designed for energy production will be much larger than the ICF targets presently studied. For long pulse irradiation of these targets at even moderate intensity ($I\lambda^2=5\times10^{14}$ W-$\mu m^2/cm^2$), intense stimulated Raman scattering (SRS) may create a hot electron environment which makes the achievement of a high density difficult. The Raman instability has a small gain coefficient and, for the instability to go strongly, there must be hundreds of wavelengths of rather homogeneous plasma for $I\lambda^2$ values typical of ICF targets. It is not surprising that up to the present, intense SRS has not been reported. Our measurements do show that SRS is much more intense at longer pulse lengths and that it can occur not only near $N_c/4$, but also at much lower densities.

The Raman instability[1-2] is a three-wave parametric process in which the laser light wave drives the Raman light wave and an electron plasma wave (epw). Energy and momentum conservation require that in a homogeneous plasma both the frequencies and wave vectors of the epw and the Raman light wave sum to equal the frequency and wave vector of the incident light wave. The epw is usually not appreciably damped by collisions, but rather loses its energy to fast electrons by wave-breaking.

Stimulated Raman scattering has been observed by others,[3-7] as well as having been predicted by computer simulations.[9-10] The earliest observation of $\omega_0/2$-light, which is a signature of resonant SRS, was reported by Bobin.[3] In Bobin's experiments a line spectrum was observed centered at $2\lambda_0$ with a 60 Å width between half-intensity points, compared to less than 30 Å width for the incident laser light. This $\omega_0/2$-light can be attributed either to resonance-Raman scattering or to linear mode conversion of the electron plasma waves produced by the $2\omega_{pe}$-instability into light waves.

J. Elazer, W. Toner, and E. R. Wooding[4] have studied the threshold behavior of the Raman instability near quarter critical density. The $\omega_0/2$ light (defined by a 5% bandwidth interference filter centered at twice the laser wavelength of 1.053 μm) was collected by the nearly f/1 target chamber lens and then focussed onto an indium antimonide detector. The threshold intensity decreased by an order of magnitude, from $\sim 10^{15}$ W/cm^2 to $\sim 10^{14}$ W/cm^2, when the focal spot diameter was increased from 50 μm to 150 μm. The laser pulselength was 2ns for both intensities, but the target material was different. The maximum conversion efficiency into $\omega_0/2$ light was about 4×10^{-7}, but the maximum laser energy at which these experiments were done was only slightly greater (less than 50% at 10^{15} W/cm^2) than the threshold energy (the experiments were done by holding the spot size and pulse length constant while varying the laser energy).

Watt[5] has seen Raman-scattering of CO_2 laser light in experiments where a 20cm length of plasma, formed in a solenoid, was irradiated by a CO_2 laser. Baldis[6] has observed $\omega_0/2$ electron plasma waves in a CO_2-irradiated plasma using Thompson scattering and, in a continuation of this work, N. A. Ebrahim, H. A. Baldis, C. Joshi, and R. Benesch[7] have directly observed the fast electrons produced at $N_c/4$. The fastest electrons (60keV) emerged in jets in the plane of polarization and at 45^0 to the density gradient. This polarization dependence indicates that the $2\omega_{pe}$ - instability was dominant. However, Ebrahim also observed fast electrons of 10 or 15 keV temperature out of the plane of polarization, suggesting Raman backscatter at lower densities.

Many 1 1/2-D particle code simulations of SRS have been done by Estabrook.[9] For example, in one simulation, 1.06 μm light at 3×10^{15} W/cm^2 was incident upon a 10 keV plasma with its initial density rising linearly from zero to 0.4 N_c in $105 \lambda_0$. Approximately 15% of the incident light was Raman backscattered.

Recent experiments at the Shiva laser facility have shown that when very large regions of plasma are irradiated by 1.06 μm light, intense

stimulated Raman scattering can occur even at the modest intensity of 5×10^{14} W/cm^2. We measured about 700 J/SR in Raman-scattered light when a tantalum disk was irradiated by 4kJ in a 2.2ns pulse. Most of this Raman scattered energy came near the end of the approximately rectangular laser pulse. Both the spectrum and the time dependence of the Raman light were measured simultaneously, but along different lines of sight.

With a third diagnostic system the Raman light intensity at one wavelength (1.8 μm) has been measured at Shiva as a function of intensity for two pulse lengths: 100 psec and 600 psec (Figure 1). As expected, at very low intensities we find the Raman light intensity to become extremely small. The really significant result, however, is that the relative Raman light intensity increased by about three orders of magnitude at 3×10^{15} W/cm^2 when the pulse length was increased from 100 to 600 psec. The spot sizes and targets were similar. Argus experiments at 600 psec with much less energy on target (typically 450 joules) will also be discussed.

We also present preliminary Raman light measurements for 5320 A green light irradiation of disk targets. The spectrum and angular distribution of the Raman light were measured by an array of photodiodes with interference filters centered at 650, 750, 800, 850, 900, and 950, and 1000 nanometers. We did not make measurements at 1.064 μm, since 10% of the 1.064 μm light enters the target chamber. The laser light was focussed by a 10 cm diameter, f/2 simple lens. Displacement of the two foci caused the 1.064 μm light intensity at the target to be extremely low; most of the light misses the target. Even though the level of Raman scattering was very small, the signal on some shots was still two orders of magnitude above our detection limit. On several of the higher intensity shots at $\sim 10^{15}$ W/cm^2, we observed a peak in the Raman light spectrum at a wavelength of 800 nm and out of the plane of polarization.

The Raman light diagnostics used in these experiments are described first (section II), followed by the Shiva experimental results (section III), and then the Argus experimental results (section IV). Our interpretations of these results are discussed in section V.

II Diagnostics

The spectrum was measured by a twenty-four element indium arsenide array cooled to liquid nitrogen temperature and operated in the photo-voltaic mode. Each element in the array was 5mm in height, 0.25mm in width, and spaced 0.35mm center-to-center from the adjacent elements. The signal from each element went into a separate charge integrator and sample-and-hold unit.

The Czerny-Turner spectrograph consisted of two six-inch focal length paraboloidal mirrors and a 75 lines/mm grating blazed for 1.8 m and used in the first order. The light was brought from the target chamber by a fifteen meter long, one millimeter diameter quartz optical fiber. The fiber optic butted against the 0.25mm wide entrance slit. A line image was formed on the InAs array by inserting a cylindrical lens in the spectrograph. The spectral range 1.48 to 2.17 μm was covered, with a dispersion of 0.03 μm/channel. The calculated dispersion was verified by bringing in light of known wavelength. For instance, the 6328Å He-Ne line in third order appears at the channel centered at 1.898 μm. We could thus quickly check that the grating angle hadn't changed; it was necessary only to remove a single filter from in front of the InAs array.

Optical filters both at the light collector on the target chamber and in front of the InAs array ensured that only Raman-scattered light was detected. The InAs array looked through a Corning 7-56 visible-light-absorbing color filter, which had been coated to be highly reflective at the laser wavelength of 1.064 μm. With the coating, essentially only light of longer wavelength than 1μm was transmitted. The light collector had a CS#4-64 near IR-absorbing filter in addition to a CS#7-56 filter. Also the target chamber window was coated to be highly reflective at 1.064 μm. The InAs array was shielded against x-rays by one-quarter inch of lead and looked through a lead-glass window.

The entire optical system was calibrated in situ, except for convenience we used a different but nearly identical fifteen meter fiber optic cable and light collector. The light collector was coupled to a blackbody source whose spectral intensity in joules/(steradian-micron)

was precisely known. The current from each element into a small resistance was then measured. Generally this current was a few nano-amperes. We also measured the linearity with a pulsed light-emitting diode, finding substantial nonlinearity.

A Molectron P5-01 fast pyro-electric detector was absolutely calibrated to give us an independent measurement of the Raman light energy and, more importantly, the time dependence. However, due to the slow time response of the pyro-electric detector, the signal had to be deconvolved. The impulse response was measured with a 50psec laser pulse and a Tektronix 7104 oscilloscope. In the actual Shiva experiments we used a different 7104 scope and P5-01 pyro-electric detector. To deconvolve the P5-01 pyro-electric signal, we first digitized the scope trace. Using an interactive computer program, we then subtracted the fiducial, did the deconvolution, and finally added the fiducial back in. The pyroelectric detector has a fast rise time of about 200 psec, but also has a long exponential tail with about a 1.5 nanosecond time constant which extends into the fiducial. To correctly separate the signal from the fiducial, we fit an exponential tail to the signal.

The absolute calibration of the detector itself was done using the Argus laser beam after the first pre-amplifier. A nominally 50-50% @ 45^0 beamsplitter provided (in reflection) the reference beam to monitor the pulse energy. We measured the exact beam-splitting ratio in place and also checked the uniformity of the beam with precision apertures. A PIN diode calibrated to 5% accuracy measured the energy density in joules/cm^2 incident upon the detector. Our calibration with a 700 psec laser pulse was close to the 17 volts/megawatt DC measurement made by Molectron. We measured 7.2 volts/megawatt for the peak; the signal pulsewidth was 1300 psec FWHM. Calculation took us the rest of the way to an overall calibration of the system (figure 3). Our calibration should be accurate to a factor of two.

Many of the Shiva measurements (figure 2) and all of the Argus measurements at 1.06 μm irradiation were made with discrete, 2mm diameter InAs detectors cooled to liquid nitrogen temperature and reverse-biased

by one volt (Figure 4). The spectral window was determined by an interference filter. The 1.064 μm light was attenuated by a factor on the order of 10^{13}, while shorter wavelength light was attenuated by at least 10^{10}. The detector was shielded from x-rays by a W-Cu housing and a Pb-SiO_2 window. Null experiments gave confidence that we were actually observing light from the target. When blocked at the vacuum window, no signal was observed on a target shot.

Two different calibration techniques were used. The most accurate calibration method was to use a blackbody source whose temperature was set to be 1200 $\pm$ 2°K (checked with a calibrated thermocouple) and whose emissivity was known to be 0.99 $\pm$ 0.01. Except for the neutral density filter attenuation, the experimental setup was duplicated. A separate calibration factor was measured for each bandpass filter.

A second, less accurate pulsed calibration method enabled us to calibrate the InAs detector alone at flux levels comparable to experimental ones, using a charge-integrating amplifier. The pulsed light source was a Q-switched Nd:Yag laser with $\lambda_0 \cong$ 1.064 μm. The spectral transmission curves for the filters and fiber optic cable were then combined with the spectral response curve for the InAs detector to obtain the overall spectral response.

III Shiva Experiments

The Raman light experiments were add-ons to several other experiments, such as experiments with 100 psec and 600 psec Gaussian pulses designed to characterize possible x-ray line sources for shadowgraphy, experiments at 600 psec Gaussian pulses using layered targets to study suprathermal electrons, and slab acceleration experiments with ≅2.2 nanoseconds rectangular pulses. The layered targets were gold-plastic-nickel-plastic disks. The laser beams always irradiated the gold side, and the gold layer was a few thousand angstroms thick. The energy in suprathermal electrons reaching the nickel layer was determined by measuring the intensity of the nickel K_α line. In the 2.2ns slab acceleration experiments, the accelerated slab was backlit by tantalum M_α x-rays. A 22X x-ray microscope, looking edge-on, imaged the

backlighting x-rays onto a streak camera. Our interest is in the backlighter tantalum disk (figure 5), which was irradiated at $5x10^{14}$ W/cm^2 with 4kJ in 2.2ns.

All the experiments were done with Shiva's upper ten laser beams. All the Shiva beams are f/6, with ten beams coming from the top and ten beams coming from the bottom. Each lens cluster (upper or lower) of ten beams consists of two nested pentagonal rings of five equally spaced beams. The inner beams axes are 9.7^0 away from the lens cluster axis, and the outer beams are 17.7^0 away. The ten upper beams were superimposed on the targets which were tilted 0^0 or $\cong 45^0$ wrt the beam cluster axis of symmetry.

The experiments designed to systematically characterize possible x-rays shadowgraph sources also offered the opportunity to study the Raman instability. Over a wide range of intensities at both 100 psec and 600 psec. These pulsewidths were measured between the half-maximum points of the nearly gaussian-shaped laser pulse. Figure 1 shows the results obtained by the discrete InAs detector, while Table I shows the results for the pyro-electric detector. No Raman light spectra were obtained for these experiments.

Figure 2 shows the location of the two diagnostics and also shows the target orientation for the 45^0 tilt angle. The disk targets were irradiated either in this orientation or at normal incidence. Both diagnostics look at 20^0 to the lens cluster axis. The discrete InAs detector and the pyro-electric detector looked at 42^0 and 62^0, respectively, to the target normal for the 45^0 target tilt or, of course, at 20^0 for the 0^0 target tilt.

All the experiments in Figure 1 were done with a 1.8 μm interference filter having an 800Å FWHM bandpass, and all, except for one marked 0^0 tilt, were done at 45^0 tilt angle. Most of the Raman light spectra we have measured show the intensity to be near it's maximum at 1.8 μm. When the pulselength was increased from 100 psec to 600 psec, the relative Raman light intensity increased by three orders of magnitude for a laser light intensity of $3x10^{15}$ W/cm^2. Also, a much higher Raman light

intensity was observed at 3×10^{15} W/cm^2 when the target was tilted 45^0 and the InAs detector looked at 42^0 to the normal than when the target was irradiated at normal incidence and the InAs detector looked at only 20^0 to the normal. This observation was confirmed by the pyro-electric detector, which has the advantage that it measures the total Raman light intensity, not just the spectral intensity at one wavelength. To see this, compare the Hf disk experiment with the two layered (HEET) disk experiments at 3×10^{15} W/cm^2 (Table I).

We also find that less Raman intensity is seen at very high intensities for the experiments described in Table I. The laser energy was limited to 4000 joules, and so the spot size had to be made much smaller for the high intensity shots. Also, of course, the coronal electron temperature is higher at high intensities. Evidently, the effects of the lessened interaction length and the greater Landau damping overcame the effect of the greater intensity.

Most of the Raman light spectra show little light near $\omega_0/2$; we believe this is most probably due to absorption. Experiments on lower Z plasmas would confirm or contradict this. Figure 6 shows a spectrum from one of the layered targets disk normally irradiated at 3×10^{15} W/cm^2 with 3.25 kJ in 600 psec. Both the spectrograph and the pyroelectric detector looked at 20^0 to the lens cluster axis. Integrating the spectrum we find $28\ ^{+28}_{-14}$ J/SR in Raman light compared to $17\ ^{+17}_{-\ 7}$ J/SR measured by the pyroelectric detector. The spectrum is extremely broad and only begins to drop off rapidly for wavelengths longer than 2.08 μm. We see the peak but cannot see to a short enough wavelength to see the Raman light intensity drop off rapidly.

In comparison, a spectrum for a 2.2ns, 4kJ, 5×10^{14} W/cm^2 tantulum disk experiment shows significant Raman scatter only at wavelengths much shorter than $2\lambda_0$; the spectrum falls off rapidly for wavelengths longer than 1.8 μm (Figure 7). This is confirming evidence for the hypothesis that the $\omega_0/2$ light is absorbed. Inverse Bremstrahlung absorption should be greater for the 2.2ns experiment than for the 600 psec experiment just described. After all, the electron

temperature should be lower (lower intensity) and the density scale length should be longer (much longer pulselength). Integrating the spectrum, we find $55\ ^{+50}_{-30}$ J/SR in Raman light. These targets were tilted 45° with respect to the lens cluster axis: the spectrograph looked at 25° to the target normal while the pyroelectric detector looked at 44° to the target normal. The pyroelectric detector on this shot measured $140^{+140}_{-\ 50}$ J/SR in Raman light.

The deconvolved signal from the pyroelectric detector (Figure 8) shows pronounced structure, as expected, since the target was irradiated in gattling-gun fashion. The ten upper Shiva beams were staggered in time by pairs, with each successive pair arriving approximately 550 psec later in time producing an rectangular irradiation pulse at the target. The gaussian-shaped pulse later in time is a fiducial signal, which is obtained from a photodiode looking at one of the incident laser beams. It is wider than the laser pulse due to the relatively slow time response of the ITT 4018 vacuum planar photodiode.

The comparison of two shots in Figure 8 proves the Raman light is most intense late in the 2.2 ns irradiation period. The laser power was also somewhat higher during this time (figure 9). The fiducials from the two shots have been overlayed so the relative timing can be compared. Neither the optical delay of the laser beam used for the fiducial nor the optical delay of the first pair of laser beams incident on the target were changed for the 2.2 ns experiments. Thus the first pair of laser beams in the 2.2 ns experiments should irradiate the target at the same time relative to the fiducial as all ten beams for the 600 psec experiment. We see that the large peak in the 2.2 ns shot occurs 2.1 ns after the peak in the 600 psec experiment. Since the last pair of beams is delayed 2.14 ns relative to the first, the Raman instability is strongest during the last period of irradiation. This result is not surprising for the plasma has the longest scale length then. It is possible that the mylar shield (see Figure 5) enhances the Raman scattering since the Raman light can be reflected from the mylar shield and go through the irradiated tantalum plasma again.

Very little Raman light was observed during the first period of irradiation. Not only was the plasma scale length smallest in that period, but also the laser intensity was only 1/2 as great then, since no energy was obtained from one beam of the first pair. The first peak arrives about 550 psec after the peak for the 600 psec shot, so we can associate it with the second pair of beams. The middle peak in figure 8 corresponds with the middle peak in figure 9.

We have irradiated six tantalum disks at 5×10^{14} W/cm^2, 2.2ns, 4000 joules, and observed about the same level of Raman scattering on all of them. The x-ray spectrum measured by the filter fluorescer has a hot 40 keV tail. The level at 50 keV is about 10^{13} keV/keV. This implies at least 40 joules are in a 40 keV Maxwellian distribution of superthermal electrons. (The actual energy in superthermal electrons will be larger, since they can lose some of their energy to fast ions rather than to collisional slowing.)

IV Argus Experiments

Low intensity experiments were carried out on 600 μm diameter, 25 μm thick gold disk targets irradiated by one beam of the Argus laser facility (figure 10). The disks were irradiated by 800 joules in 950 psec Gaussian pulses focused to a spot of about 425 μm minor diameter, 500 μm major diameter, except for the case of the Ba $(NO_3)_2$ disk target. This disk was irradiated at about 1/3 the energy with a correspondingly smaller spot size. The intensity was always about 5×10^{14} W/cm^2. The disks were tilted 30^0 in the plane of polarization and the light collector always looked within 11^0 of the target normal. This was necessary because the light at frequency $\omega_0/2$ is generated very near its critical density and refraction causes it to emerge at an angle very near to the normal regardless of what its direction was when it is generated in the plasma.

Each point in Figure 10 represents the result of one such target experiment. The bandpass interference filter in front of the InAs detector was changed between shots to get the spectral shape. The width of each point is given by the FWHM bandpass of the interference filter.

Different materials were irradiated because the Raman light measurements were secondary diagnostics on an experimental series on various Z disk targets designed to characterize x-radiography sources. All the materials used had at least a moderately high Z. The spectrum is highly peaked and extends to the red beyond $2\lambda_o$. We did not make any measurement for wavelengths longer than 2.2 μm. The signals at 1.8 μm and 2.0 μm could be caused by leakages of the observed strong signal near $2\lambda_o$ through these bandpass filters.

The $\omega_o/2$ light spectrum extends to the red beyond 2.128 μm ($2\lambda_o$) due to the Bohm-Gross shift, as first explained by Kruer[11]. If one solves the dispersion relations for the two light waves and the electron plasma wave to find the density at which the Raman light wave is exactly at its critical density, one finds this density is below $N_c/4$ and that the Raman light wave thus has a wavelength longer than $2\lambda_o$. These dispersion relations are:

electron plasma wave $\omega^{*2} \approx \omega_{pe}^2 + 3v_{te}^2 k^{*2}$ for $3v_{te}^2 k^{*2} \ll \omega_{pe}^2$

Eq. (1) Raman light wave $\omega_R^2 = \omega_{pe}^2 + c^2 k_R^2$

incident light wave $\omega_o^2 = \omega_{pe}^2 + c^2 k_o^2$

where ω_{pe} is the electron plasma frequency, $v_{te} = \sqrt{kT_e/m_e}$ is the electron thermal velocity, and ω^* and k^* are the angular frequency and wavenumber of the electron plasma wave, respectively. One sets $\omega_R = \omega_{pe}$ and $\omega^* = \omega_o - \omega_R$ to find

Eq. (2) $$\omega_o - \omega_R = \sqrt{\omega_R^2 + 3v_{te}^2 k^{*2}}$$

For $k^* = \sqrt{8/9}\,\frac{\omega_o}{c}$, we get:

Eq. (3) $$\frac{\lambda_R - 2\lambda_o}{\lambda_R} = \frac{\theta_e}{227\ \text{keV}}$$

where θ_e is the electron temperature in keV. This shift is about 1/2% per keV electron temperature.

The threshold for stimulated Raman scattering is expected to be lowest near the quarter critical density for two reasons: first, the group velocity of the Raman light wave is near zero there so the instability can become absolute rather than convective; and secondly, for backward scattering the phase velocity of the Raman light wave is highest there, resulting in the least Landau damping. The phase velocity of the electron plasma wave (epw) at $N_c/4$ is near $c/\sqrt{3}$. An electron moving at this speed has a kinetic energy of 115 keV. Thus, Raman light generated near its critical density produces electrons with energies of order 100 keV. In Figure 11 the wavebreaking energy for Raman backscatter is plotted versus the electron density for several values of θ_e. The wavebreaking energy is the relativistic kinetic energy of an electron moving at the epw phase velocity v_0. Higher θ_e increases v_0. The Bohm-Gross approximation is only valid if $k*\lambda_{De} \ll 1$, where $\lambda_{De}=v_{te}/\omega_{pe}$ is the electron Debye length. Figure 11 thus becomes wrong at low electron densities. At higher θ_e, Raman scattering can occur only at lower densities:

Eq. (4) $$\frac{N_e}{N_c} \leq \left(\frac{1-\xi}{1+\sqrt{1-\xi+\xi^2}}\right)^2$$

where $\xi = 3v_{te}^2/c^2$ is a dimensionless parameter proportional to the electron temperature. In Figure 12 the wavebreaking energy is plotted for side- and forward-scatter as well as backscatter.

C.S. Liu[1] shows the condition for absolute instability in an inhomogeneous plasma to be

Eq. (5) $$\left(\frac{v_o}{c}\right)^2 > \frac{4}{(k_o L)^{4/3}}$$

where L is the local density gradient defined by

Eq. (6) $$\frac{1}{L} = \frac{1}{N_e}\frac{dN_e}{dx}$$

Here k_0 is the wavenumber of the incident light in vacuum, and v_0 is the peak oscillatory velocity of the electron in the incident light field. The threshold condition given here actually agrees with Liu's, given by Eq. I-31 on page 133 of reference 1, despite a seeming discrepancy by a constant factor. Liu's v_0 is actually half the peak oscillatory velocity (see Eqs. I-13 and I-19). The peak oscillatory velocity for linearly polarized 1.064 m light is given by:

Eq. (7) $$\left(\frac{v_0}{c}\right)^2 = \frac{I\lambda^2}{1.37 \times 10^{18}\ W\text{-}\mu m^2/cm^2}$$

Simulations[11] indicate L~150 μm, so that we were close to threshold for I = 5 x 10^{14} W/cm^2. Of course, the peak intensity of the beam in hot spots may be a factor of several higher than this average intensity.

At light intensities of 10^{16} and 10^{17} W/cm^2, the spectral intensity of the Raman-scattered light increased not only near the degeneracy frequency $\omega_0/2$, but even more so at higher frequencies (Table II). The Raman light intensity at 1.6 μm and 1.8 μm is comparable to that at 2.13 μm. All these measurements were made with the Raman light collector in the plane of polarization of the incident light. However, stimulated Raman scattering should have the maximum gain when the scattering plane is orthogonal to the plane of polarization. The electric vector of the Raman light would then be parallel to the electric vector of the incident light. Since the growth rate of the Raman instability is proportional to the dot product of the two electric vectors, the out-of-plane scattering is expected to occur preferentially. We have not yet made out-of-plane measurements.

For the experiments at 10^{16} W/cm^2, the gold disks were tilted 30^0 in the plane of polarization and toward the Raman light collectors, so that they looked nearly normal to the target surface. However, the shots at 10^{17} W/cm^2 were done at normal incidence, so the Raman light collectors were looking 25^0 away from the incident beam and in the plane of polarization.

Raman light measurements have also been made for the 5320Å green light experiments carried out at Argus (figure 13). These measurements were made with an array of silicon PIN 6/LC photodiodes, made by United Detector Technology. Calibrations for the photodiode sensitivities have not been done yet; we used the manufacturer's nominal sensitivity curve. The diodes were reverse-biased by 45 volts, and the signals went into charge integrators. The green light was blocked with Schott RG610 sharp red cut-on color filters. The interference filters have a 125Å FWHM nominal bandpass and are fully blocked to 0.01%. X-rays were shielded against by using a 1/8 inch thick lead-equivalent-thickness lead glass window and by making the photodiode housing out of a tungsten alloy. The experimental results shown in figure 13 are atypical in that usually the Raman light signals were much smaller. However, a large polarization dependence was always seen. The gold disk was irradiated at about 10^{15} W/cm^2 with 32 joules in about 600 psec. The lens was f/2, and the laser light was linearly polarized. The disk was tilted 10^0 in the plane of polarization. One ring of photodiodes looked in the plane of polarization and another ring of photodiodes looked out of the polarization plane. Most of the diodes looked at light coming back at 25^0 or 30^0 to the laser beam. The angles θ_N in figure 13 specify how far away from the target normal the photodiode looked. The data shows that the Raman scattering occurs at very low electron density, and that there is an extremely strong polarization dependence. Such a strong polarization dependence would only be expected for side-scatter.

V Comparison With Theory

Here we present our conclusions about where the Raman scattering is occurring, whether back- or side-scatter predominates, and what the growth lengths are.

The coupled mode equations for Raman scatter are 1-2

Eq. (8)
$$\left(\frac{\partial^2}{\partial t^2} + 2\nu_R \frac{\partial}{\partial t} - c^2\nabla^2 + \omega_{pe}^2\right)\vec{A}_1 = -\frac{4\pi e^2}{m_e}(n_e \vec{A}_1)_{\text{transverse}}$$

$$\left(\frac{\partial^2}{\partial t^2} + 2\nu_L \frac{\partial}{\partial t} - 3v_e^2\nabla^2 + \omega_{pe}^2\right) n_e = \frac{n_0 e^2}{m_e^2 c^2}\nabla^2(\vec{A}_0 \cdot \vec{A}_1)_{\text{longitudinal}}$$

where ω_{pe} is the electron plasma frequency, n_0 is the equilibrium electron density, n_e is the electron density fluctuation caused by the electron plasma wave, m_e is the electron rest mass of 0.911×10^{-27} grams, e is the electric charge of -4.8×10^{-10} statcoulombs, A_0 and A_1 are the vector potentials for the incident and Raman-scattered wave, respectively, c is light speed, and v_{te} is the electron thermal velocity defined by Eq. 1. Units are unrationalized CGS, and the Coulomb gauge is used.

We assume the plasma is only weakly inhomogeneous and that the electron plasma wave is strongly damped. By weakly inhomogeneous and strongly damped, we mean that the electron plasma wave is locally driven and the Raman instability is convective or spatially growing rather than absolute or temporally growing. We can then solve for the amplitude n_e of the electron plasma wave anywhere just knowing the local fields A_0 and A_1. We assume the fields to have the local harmonic dependence:

Eq. (9)
$$\vec{A}_0(\vec{r},t) = Re\left(\vec{e}_0 \tilde{A}_0 \exp\left[-i(\omega_0 t - \vec{k}_0 \cdot \vec{r})\right]\right)$$
$$\vec{A}_1(\vec{r},t) = Re\left(\vec{e}_R \tilde{A}_1 \exp\left[-i(\omega_R t - \vec{k}_R \cdot \vec{r})\right]\right)$$
$$n_e(\vec{r},t) = Re\left(\tilde{n}_e \exp\left[-i(\omega^* t - \vec{k}^* \cdot \vec{r})\right]\right)$$

The tilda denotes a complex quantity. An asterisk superscript appearing on any complex quantity (which the polarization vectors are), denotes the complex conjugate. The fields $\tilde{A}_0$, $\tilde{A}_1$ and $\tilde{n}_e$ are assumed to be slowly varying functions of position and time. We then obtain

Eq. (10)
$$\tilde{n}_e(\omega^*, k^*) = \frac{-k^{*2} \tilde{A}_0^* \tilde{A}_1 / 2 \; \vec{e}_0^* \cdot \vec{e}_R}{\omega_{BG}^2(k^*) - \omega^{*2} - 2i\nu_L\omega^* - 6i\nu_{te}^2 \, Im\, k \, \vec{n}^* \cdot \vec{n}_R}$$

The quantity Imk is the amplitude growth per unit distance for the Raman light wave. It's effect on the resonance denominator in Eq. 10 is usually small and we will drop it. The vectors $\vec{e}_0$ and $\vec{e}_R$ are unit electric polarization vectors, while $\vec{n}_R$ and $\vec{n}^*$ are unit vectors in the

direction of k_R and k^*, respectively. The angular frequency $\omega_{BG}(k^*)$ is the Bohm-Gross frequency for an electron plasma wave with wave number k^* (see Eq. 1). One finds the growth in a wavelength to be from Eq. (8)-(10)

$$\text{Eq. (11)} \quad \frac{1}{\tilde{A}_1}\frac{\partial \tilde{A}_1}{\partial(s/\lambda_c)} = \lambda_c \operatorname{Im} k = \frac{\pi}{4}\left|\vec{e}_c\cdot\vec{e}_R^{\,*}\right|^2\left(\frac{k^{*2}}{k_c k_R}\right)\left(\frac{v_0}{c}\right)^2 \times \left(\frac{-i\omega_{pe}^2}{\omega_{BG}^2(k^*)-\omega^{*2}-2i\nu_L\omega^*}\right)$$

Here s is the path length along the Raman light wave ray path and v_0 is the unswelled oscillatory velocity.

If the electron plasma wave is resonantly driven, the growth is

$$\text{Eq. (1c)} \quad \frac{1}{\tilde{A}_1}\frac{\partial \tilde{A}_1}{\partial(s/\lambda_c)} = \frac{\pi}{8}\left|\vec{e}_R^{\,*}\cdot\vec{e}_c\right|^2\left(\frac{k^{*2}}{k_c k_R}\right)\left(\frac{\omega_{pe}}{\omega^*}\right)\left(\frac{v_0}{c}\right)^2$$

This result is a factor of two lower than that of Forslund, Kindel, and Lindman[10], but their paper assumed circularly polarized light rather than linearly polarized light and defined v_0 as the circular velocity of the electrons. Their gain coefficient is larger since two orthogonal, linear polarized electric fields drive the same electron plasma wave.

Our data suggests, as will be shown later, that Raman side-scatter is at least as important as Raman back-scatter. Looking at the expression for the growth rate, one would at first think back-scatter would predominate, due to the factor $k^{*2}/(k_0 k_R)$. Back-scatter gives the largest electron plasma wave number k^* and the smallest Raman light wave number k_R. For side-scatter though, the epw has a higher phase velocity and is consequently less Landau-damped. Also, for a normally irradiated disk, side-scatter may have a much longer interaction length than back-scatter. The epw will cease to be resonantly driven if the electron density changes by a fractional amount $\Delta N_e/N_c$ about equal to twice the fractional Landau damping ν_L/ω_{pe}. By propagating

transversely to the density gradient, the Raman light wave may see an almost constant electron density. Of course, this is complicated by refraction of the Raman light wave, the finite spot size, curvature of the plasma density contours, and plasma turbulence.

An estimate of the intensity e-folding growth length can now be made. Assuming side-scatter at one-tenth critical density, we find the intensity gain coefficient to be:

Eq. (13) $$\frac{1}{|\vec{A}_1|^2}\,\frac{\partial|\vec{A}_1|^2}{\partial(s/\lambda_c)} \cong 1.2\left(\frac{\omega_{pe}}{\omega_L}\right)\left(\frac{I\lambda^2}{1.37\times10^{18}\ W\text{-}\mu m^2/cm^2}\right)$$

The last expression in parentheses equals v_e^2/c^2. The Raman gain coefficient is small and hundreds of wavelengths of underdense plasma are typically required for the instability to go.

The Raman light spectra strongly suggests the Raman light we observed originated from side-scatter. Figure 14 compares the solutions to the dispersion equations for side- and back-scatter, for θ_e=5keV. We believe θ_e can't be much below 5keV in the 5 x 10^{14} W/cm^2, 2.2ns experiments. Each point represents a computer solution of the dispersion relations for the three waves, demanding conservation of frequency and wave vector. Instead of the Bohm-Gross approximation to the epw dispersion relation given by Eq. (1), the exact plasma dispersion integral[12] has been used to calculate a complex angular frequency ω^* for the epw, given the real wave number k*. The computer solution demands the real part of ω^* plus the real part of ω_R sum to equal ω_0. This isn't quite correct. For a steady-state solution, the angular frequencies will be real, and it will be the wave vectors which have an imaginary part. Drake[10], et. al. give the correct, but much more complicated, solution to this problem. The crux of our argument for the occurrence of Raman side-scatter is that back-scattered Raman light with wavelengths as short as observed would have to originate at an extremely low density. Even for a 5keV background electron temperature, the electron plasma waves would be strongly damped. If the Raman light

had a wavelength λ_R equal to 1.75 μm, back-scatter would have the Raman instability occurring at 0.066 critical density and would have the wave-breaking energy be 18keV. The fractional Landau damping would be $\nu_L/\omega_{pe} = 0.25$ and the intensity e-folding growth length would be 340 m for $I = 5 \times 10^{14}$ W/cm^2 and $\lambda_0 = 1.064$ μm. Since our spot size in the 2.2ns backlighter experiments was only 600 x 850 μm, it would seem the Raman instability would be below threshold for back-scatter at $\lambda_R = 1.75$ μm. For side-scatter, 1.75 μm Raman light originates at 0.104 critical density. The fractional Landau damping is only $\nu_L/\omega_{pe} = 0.026$ and about 50 μm of plasma are needed for an intensity e-folding. Five or ten intensity e-folding lengths are certainly possible in this case. The plasma the Raman light wave passes through must be rather homogeneous, however. The electron plasma wave will be nearly resonantly driven only if $\Delta N_e/N_c \leq 2\nu_L/\omega_{pe}$. Thus, the electron density would have to be constant to ± 6% over a distance of 250 to 500 μm. It's difficult to see how this can be possible unless it is side-scatter.

The effect of refraction must of course be considered. For the scale lengths of many hundreds of microns expected in the 2.2ns, 5×10^{14} W/cm^2 experiments, refraction turns out to be negligible for densities below a tenth critical density.

The radius of curvature ρ of a Raman light ray propagating transversely to the density gradient is given by:

Eq. (14) $$\frac{1}{\rho} = \frac{d}{dx}\sqrt{1 - \frac{N_e}{N_c(\lambda_R)}}$$

where $N_c(\lambda_R)$ is the critical electron density for light of wavelength λ_R and x is distance along the density gradient. If the ray bending angle over the distance $\ell/2$ (figure 15) is small, to good approximation we have

Eq. (15) $$\Delta x \approx \frac{\ell^2}{8\rho}$$

We also then have:

Eq. (16) $$\frac{\Delta N_e}{N_e} \approx \frac{\Delta x}{L} \approx \frac{\ell^2}{8\rho L}$$

If we now set $\Delta N_e/N_e$ equal to $2\nu_L/\omega_{pe}$, we find:

Eq. (17) $$\ell = \sqrt{32\left(\frac{\nu_L}{\omega_{pe}}\right)\left(\frac{N_c(\lambda_R)}{N_e}\right)}\left[1-\frac{N_e}{N_c(\lambda_R)}\right]^{1/4}$$

Picking λ_R = 1.75 μm, N_e = 0.104 $N_c(\lambda_0)$, ν_L/ω_{pe}=0.03 and L = 500 μm, the maximum interaction length ℓ turns out to be 850 μm. The radius of curvature ρ of the Raman light ray turns out to be three millimeters. It of course doesn't matter whether it is refraction causes that the Raman light to curve away from the plasma or it is the plasma density contours that curve away from the Raman light ray. Either way the Raman light ray still leaves the interaction region. The value for to use in Eq. 16 is the sum of the two curvature radii.

VI Conclusion

The Shiva experiments demonstrate that the Raman instability can be several per cent efficient even at 5×10^{14} W/cm^2 for one micron laser light when the plasma and laser spot size are sufficiently large. We have also found experimentally that Raman scattering can occur not only near quarter critical density, but also at much lower densities. Indeed, little Raman light may be seen near $\omega_0/2$ simply due to absorption.

The $2\omega_{pe}$ instability also produces energetic electrons and also is expected to become more significant with larger plasmas and laser spot sizes. We have not looked for the $2\omega_{pe}$ instability in these experiments, but it certainly should be studied in future experiments. K. G. Estabrook, W. L. Kruer, and B. F. Lasinski[14] have done a two-dimensional particle code simulation in which the plasma went from 0.195 to 0.235 N_c in $25\lambda_0$ and the background electron temperature was 3keV. One micron laser light was normally incident with an intensity of 3×10^{15} W/cm^2. The $2\omega_{pe}$ - instability caused a large fraction of the 32% absorption.

The underdense plasma at and below quarter critical density promises to be extremely interesting to plasma physicists, but only a curse to laser fusion. We hope it ceases to be a problem with shorter wavelength laser light. At shorter wavelength, the Raman gain coefficient will be smaller and the collisional damping it undergoes will be much higher. Estabrook[13], et. al., pointed out that even in an infinite homogeneous plasma slab, the Raman instability may be stabilized by inverse Bremstrahlung absorption.

Acknowledgements

Many people at Argus and Shiva worked to field these diagnostics, especially Bob Reed and Dave Walton of the Target Diagnostics group. The design is the work of Bill Laird in the Mechanical Engineering group. Discussions with Bill Kruer and Kent Estabrook in the Plasma Theory group were important both in initially stimulating these experiments and in determining what to look for. The Experimental Program management, especially H. Ahlstrom and K. Manes, greatly encouraged these experiments. I thank Mike Campbell for the interest and encouragement which helped motivate the Argus experiments, and also for his help in planning these experiments.

This work was performed under the auspices of the U.S. Department of Energy by Lawrence Livermore National Laboratory under contract No. W-7408-ENG 48.

References

1. C. S. Liu in Advances in Plasma Physics, edited by Albert Simon and W. B. Thompson (Wiley, New York, 1976), vol. 6, p. 121.
2. C. S. Liu, M. N. Rosenbluth, and R. B. White, Phys. Fluids 18, 1002 (1975).
3. J. L. Bobin, M. Decroisett, B. Meyer, Y. Vitel, Phys. Rev. Lett. 30, 594 (1973).
4. J. Elazar, W. Toner, and E. R. Wooding, pages 3.10 to 3.13 of the Annual Report to the Laser Facility Committee 1980, Rutherford Laboratory report RL-80-026 (Laser Division).
5. R. G. Watt, R. D. Brooks, and Z. A. Pietrzyk, Phy. Rev. Lett. 41, 271 (1978).
6. H. A. Baldis, J. C. Samson, and P. B. Corkum, Phys. Rev. Lett. 41, 1719 (1979).
7. N. A. Ebrahim, H. A. Baldis, C. Joshi, and R. Benesch, Phys. Rev. Lett. 45, 1179 (1980).
8. Chan Joshi, Chris Clayton, Ahio Yasudo, and Frank Chen have reported seeing Raman scatter in a pre-ionized plasma.
9. W. L. Kruer, K. G. Estbrook, B. F. Lasinski, and A. B. Langdon, Phys. Fluids 23, 1326 (1980).
10. D. W. Forslund, J. M. Kindel, and E. L. Lindman, Phys. Fluids 18, 1017 (1974); D. Biskamp and H. Welter, Phys. Rev. Lett. 34, 313 (1975); W. L. Kruer, K. G. Estabrook, and K. H. Sinz, Nuc. Fusion 952 (1973); W. Manheimer and H. Klein, Phys. Fluids 17, 1889 (1974); B. I. Cohen, A. N. Kauffman, and K. M. Watson, Phys. Rev. Lett. 29,581 (1972).
11. M. D. Rosen of Lawrence Livermore National Laboratory, private communication.
12. J. F. Drake, P. K. Kaw, Y. C. Lee, G. Schmidt, C. S. Liu, and Marshall N. Rosenbluth, Phys. Fluids 17, 778 (1974).

13. J. O. Jackson, J. Nucl. Energy, Part C: Plasma Phyics, vol. 1, pp. 171-189 (1960). The program which evaluated the plasma dispersion integral in this paper was written by Kent Estabrook.

14. K. G. Estabrook, W. L. Kruer, and B. F. Lasinski, "Heating by Raman Back and Forward Scatter, Lawrence Livermore Laboratory UCRL-84270 Rev. II, accepted for publication by Physical Review Letters.

Figure Captions

Figure 1 Raman light measurements made at the Shiva laser facility with an LN-cooled indium arsenide detector. The targets were tilted 45^0 (except for the point marked 0^0) to the lens cluster axis and viewed at 42^0 to the target normal and 20^0 to the lens cluster axis.

Figure 2 Location of the Raman light diagnostics for all the Shiva experiments. The target orientation and the indicated viewing angles with respect to the target normal are correct only for the backlighter experiments done at 45^0 tilt angle.

Figure 3 Experimental set-up at Shiva for the P5-01 pyro-electric detector looking at Raman-scattered light. Only the pyro-electric detector at $\theta=20^0$, $\theta=126^0$ in the upper lens cluster was used in the experiments reported here. The inset at the upper right is the transmission of the optics in the light collector.

Figure 4 Experimental setup at Argus for the liquid nitrogen cooled, indium arsenide detector looking at the Raman-scattered light. Filters identified by numbers are: 1- Visible-light-absorbing, Corning 7-56 filter. Transmittance for $\lambda < 0.75\ \mu m$ is $< 10^{-4}$; 2- Lead glass; 3- Near IR absorbing, Corning 4-64 filter with a 99% reflective coating at 1.064 μm. Transmittance without the reflective coating for $0.65\ \mu m < \lambda < 1.1\ \mu m$ is 10^{-3}; 4- Bandpass interference filter with nominal 800 A half-width and blocked to better than 10^{-3}.

Figure 5 Backlighter target used in the 2.2ns slab accelerationexperiments. The Raman light experiment was an add-on. The tantalum disk was irradiated at 5×10^{14} W/cm^2 for 2.2ns with the upper ten laser beams while the glass disk was irradiated for 600 psec with the lower ten beams. Our interest is in the tantalum disk, which backlit the slab with the Ta M_α x-ray line.

Figure 6 Raman light spectrum from a gold-plastic-nickel-plastic disk irradiated at Shiva with the upper ten beams normally incident. The disk was irradiated at 3.3×10^{15} W/cm^2 with 3.25kJ in 600 psec. The laser spot size was 460 μm diameter; the beams were almost completely overlapping. The target was viewed at 20^0 to the target normal.

Figure 7 Raman light spectrum for a tantalum disk tilted 45^0 and irradiated with the upper ten beams of Shiva. The disk was irradiated at 4.6×10^{14} W/cm^2 with 4100 joules incident in 2.2ns. The laser beams were staggered in time so that the individual 600 psec FWHM pulses added up to give nearly constant irradiation. The target was viewed at 25^0 to the target normal and at 20^0 to the lens cluster axis.

Figure 8 Deconvolved signals from a fast P5-01 pyro-electric detector shows Raman light most intense lat. in the laser pulse. The narrow signal on the left is shown for a time reference. The first beams irradiated the target in the 2.2ns experiments at the same time relative to the fiducial as did all ten beams in the 600 psec experiment shown for reference. The fiducial signals on the right have been overlayed using their half-maximum points.

Figure 9 Calculated time dependence of the laser power on target for the 2.2ns, 5×10^{14} W/cm^2, 4100 joule tantalum disk experiment described in the text. The ten beams were staggered in time by pairs. Each successive pair was delayed in time by about 550 psec. The time scale is defined so the peak power of the first pair is at t=0. The power is low early in the pulse because one beam of the first pair failed. The actual beam energies and delay times were used in calculating this curve.

Figure 10 Spectrum of the Raman light obtained at Argus for disks irradiated at 5×10^{14} W/cm^2 with 800 joules in 1ns. The target tilted 30^0 in the plane of polarization to the f/2 beam. The indium arsenide detector always looked within 11^0 of the target normal. Each point represents a separate experiment, and the barium disk experiment was done at 1/3 the energy, but at the same intensity.

Figure 11 Wave breaking energy of the electron plasma wave driven by Raman backscatter as a function of the electron density for several values of the electron temperature. The Bohm-Gross approximation has been made, so the two curves with $T_e > 0$ are not correct for low electron density, where $k^* \lambda_{De} \gtrsim 1$.

Figure 12 Wave breaking energy of the electron plasma wave driven by the Raman instability in a cold plasma.

Figure 13 Raman light spectrum for a gold disk irradiated at about 10^{15} W/cm^2 with 32 joules in about 600 psec. Laser wavelength was 5320A (all other experiments reported here were done at 1.064 μm). The spot size was about 50 by 100 μm. The disk was tilted 10^0 in the plane of polarization. Focussing lens was f/2. Each point represents a photodiode measurement with an interference filter of nominally 125A FWHM bandpass.

Figure 14 Raman light wavelength for both side- and back-scatter as a function of electron density for θ_e=5keV. Each point represents a computer solution using the plasma dispersion function rather than the simple Bohm-Gross approximation.

Figure 15 Geometry for the Raman light ray refracting in an inhomogeneous planar plasma.

Table Captions

Table I - Pyro-electric detector measurements made at Shiva of the Raman light intensity.

Table II- Raman light measurements made in high intensity experiments at Argus. The indium arsenide detector looked at an angle θ_N away from the target normal.

SHIVA RAMAN LIGHT EXPERIMENT RESULTS FOR THE BACKLIGHTING SERIES

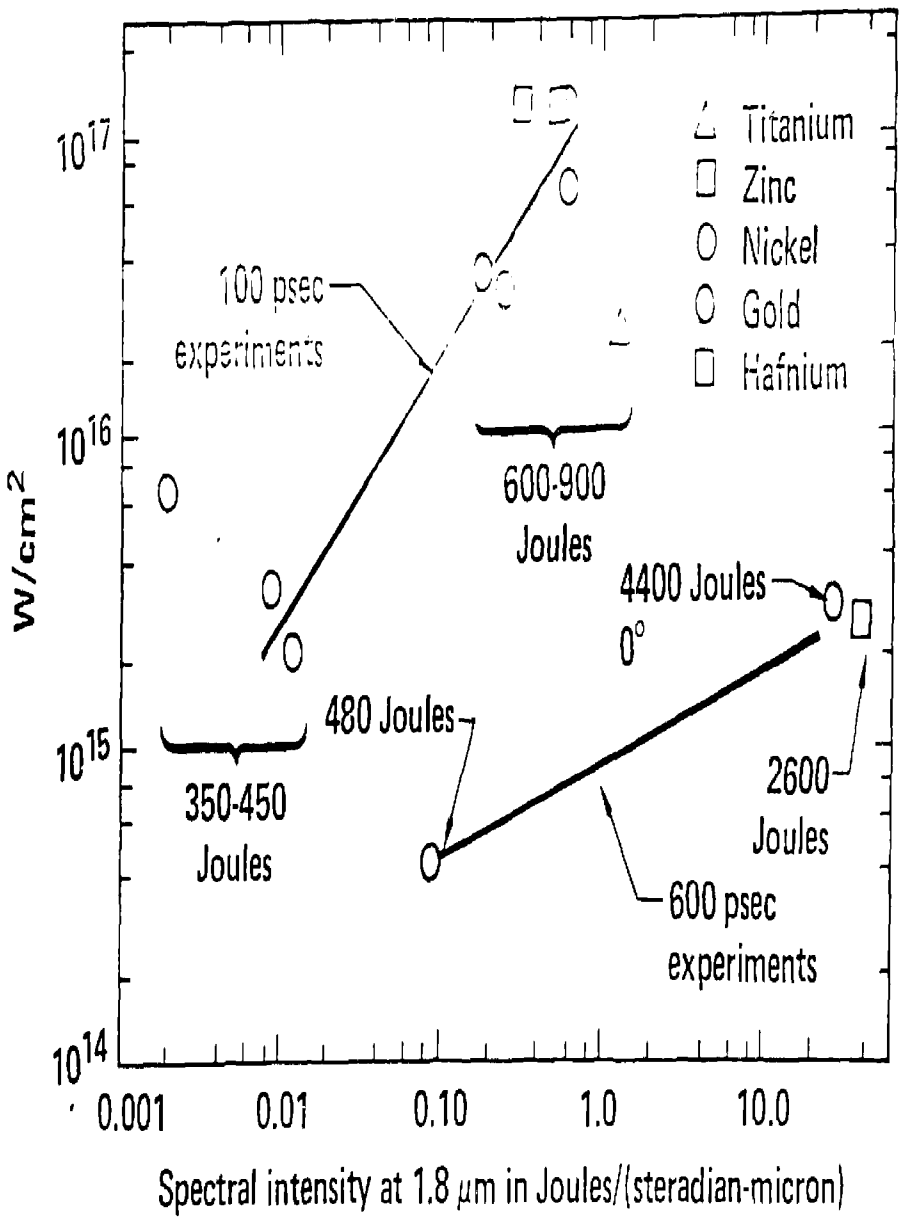

02-30-0980-2972

LOCATION OF THE RAMAN LIGHT DETECTORS IN THE SHIVA BACKLIGHTING EXPERIMENTS

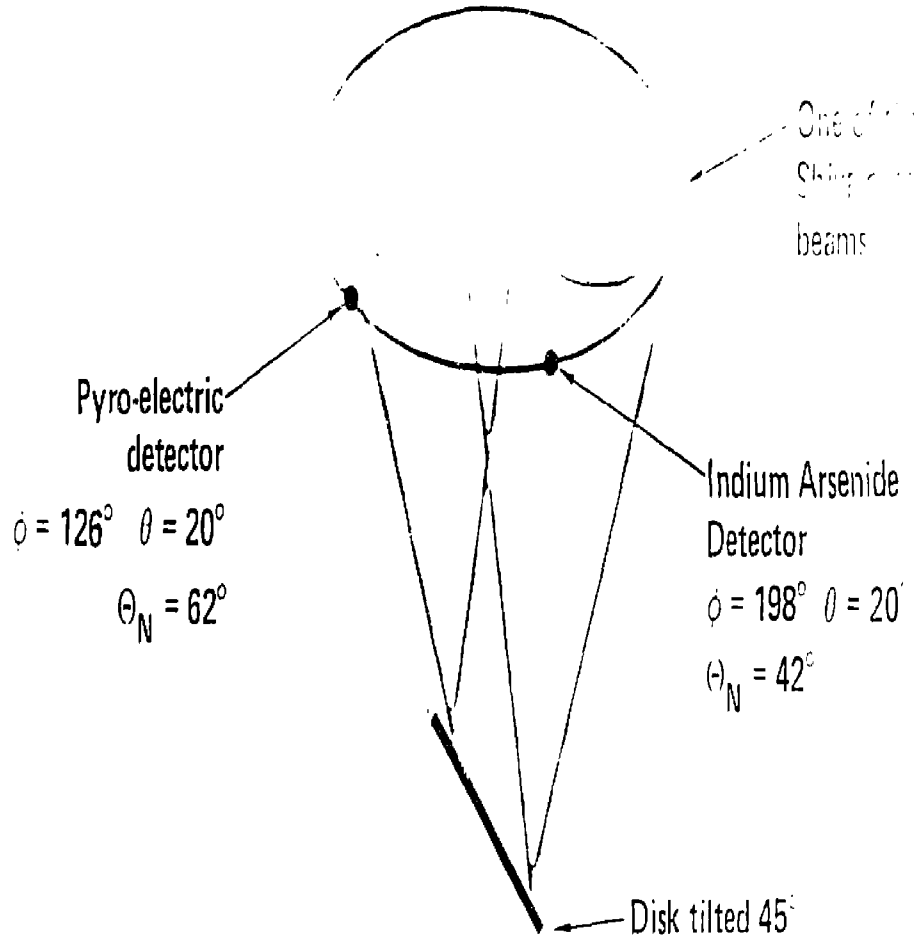

02-30-0980-2974

10 80

Figure 2

SHIVA PYROELECTRIC DETECTORS

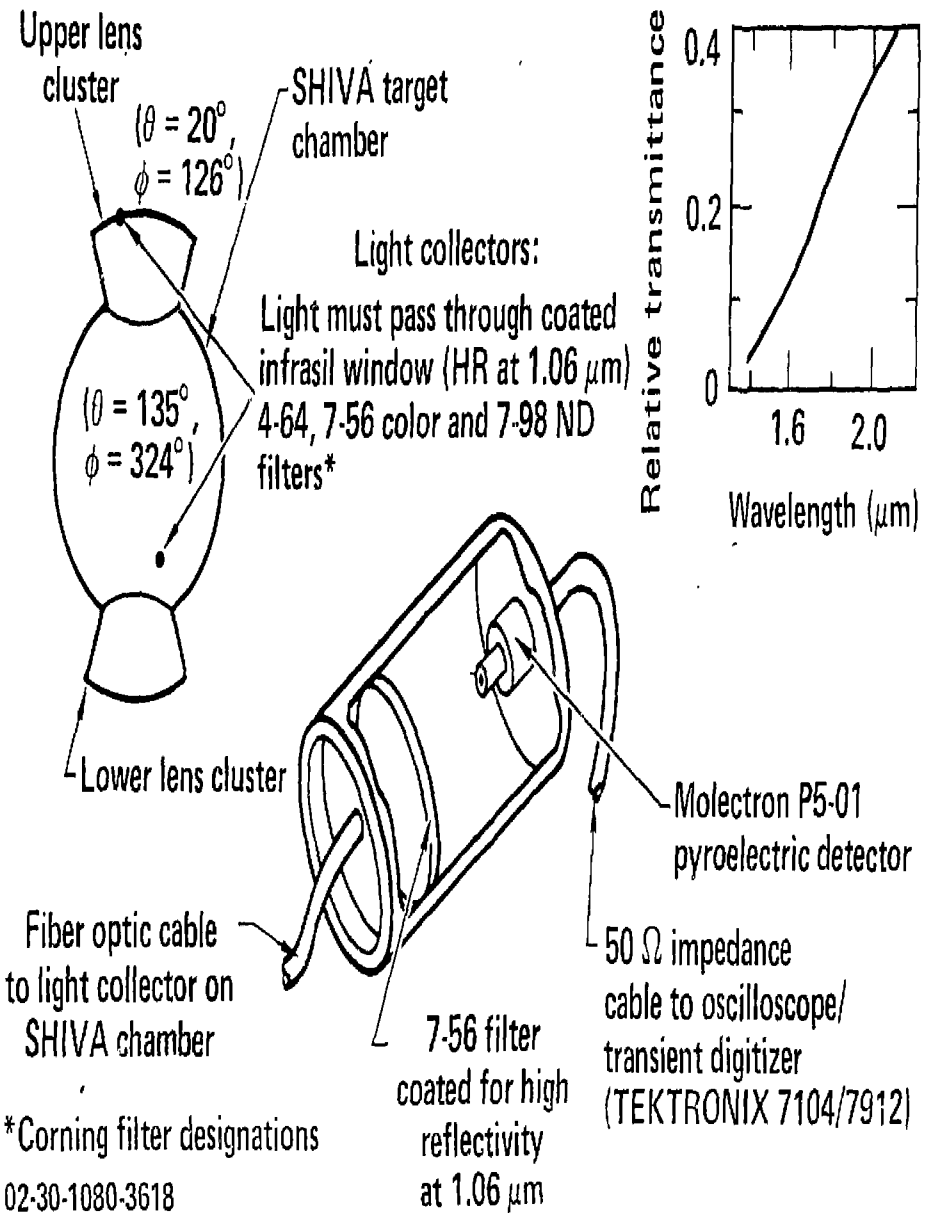

Figure 3

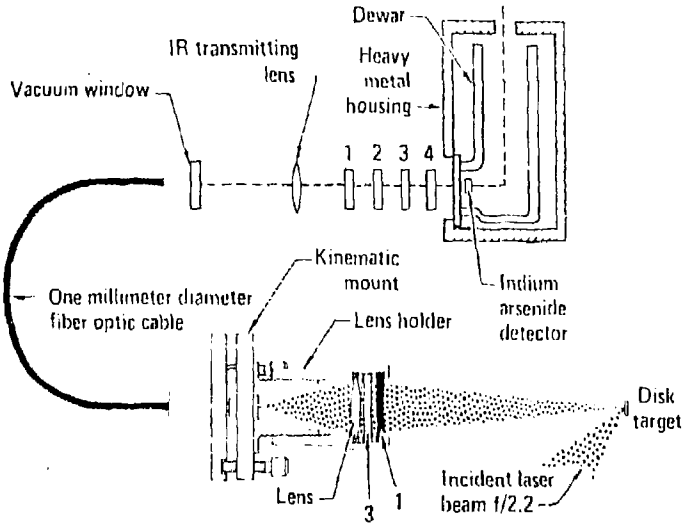
Dewar
IR transmitting lens
Heavy metal housing
Vacuum window
1 2 3 4
Kinematic mount
One millimeter diameter fiber optic cable
Lens holder
Indium arsenide detector
Disk target
Incident laser beam f/2.2
Lens
3
1

Figure 4

ENTERPRISE X-RAY BACKLIGHTING TARGET FOR SLAB ACCELERATION EXPERIMENTS

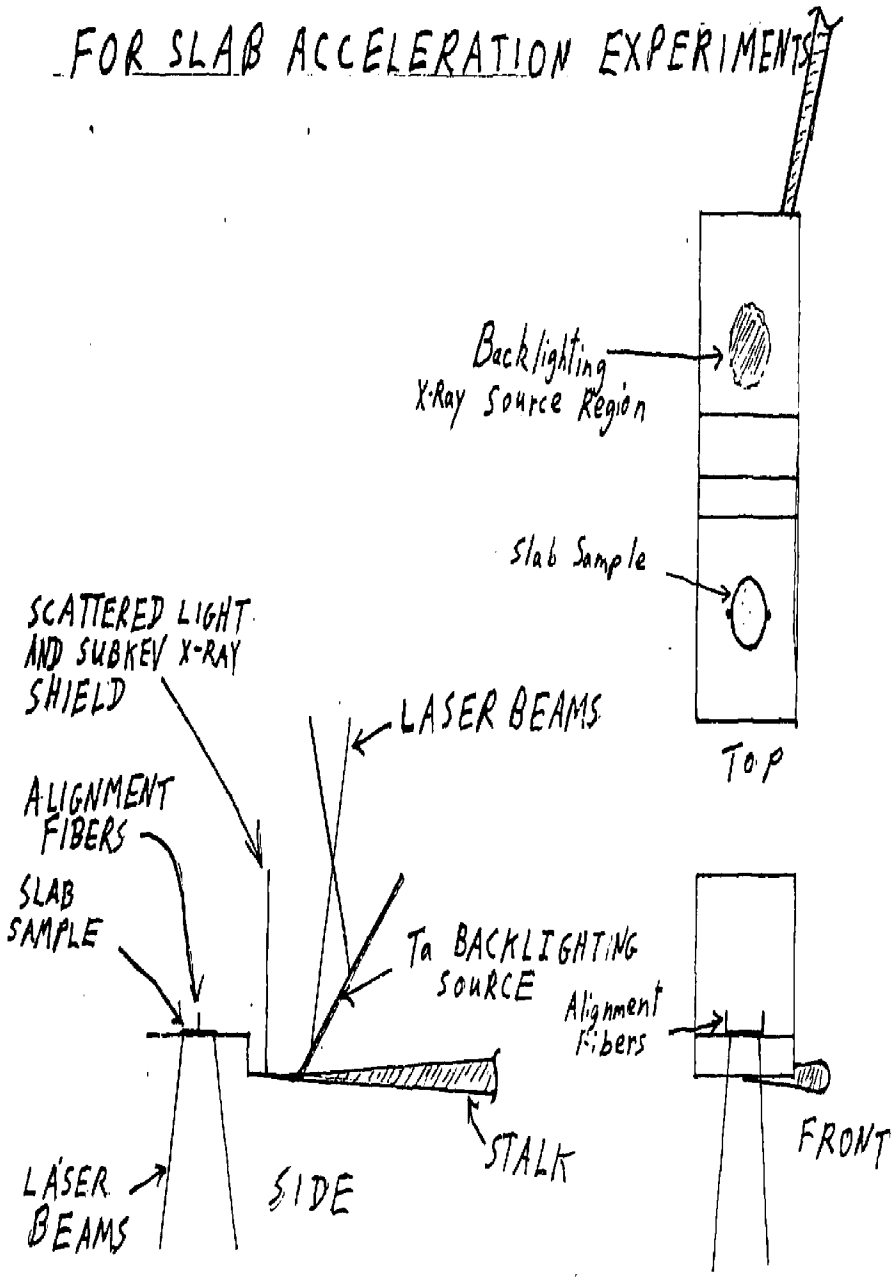

Figure 5

RAMAN LIGHT SPECTRUM FROM SHIVA GOLD DISK EXPERIMENT

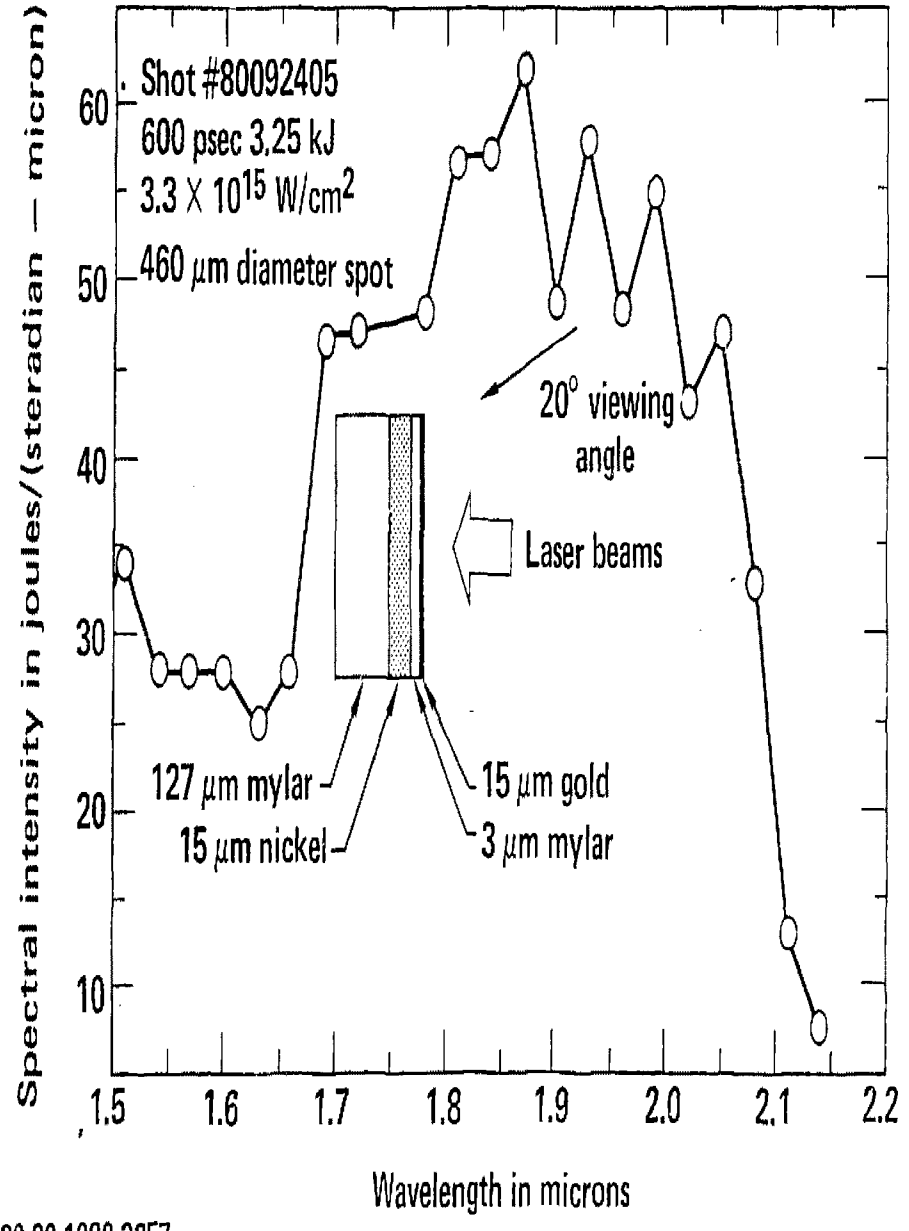

20-90-1080-3257

Figure 6

RAMAN LIGHT SPECTRUM FOR A TANTALUM DISK IRRADIATED WITH 4100 J IN A 2.2 NS PULSE AT 4.6×10^{14} W/cm^2

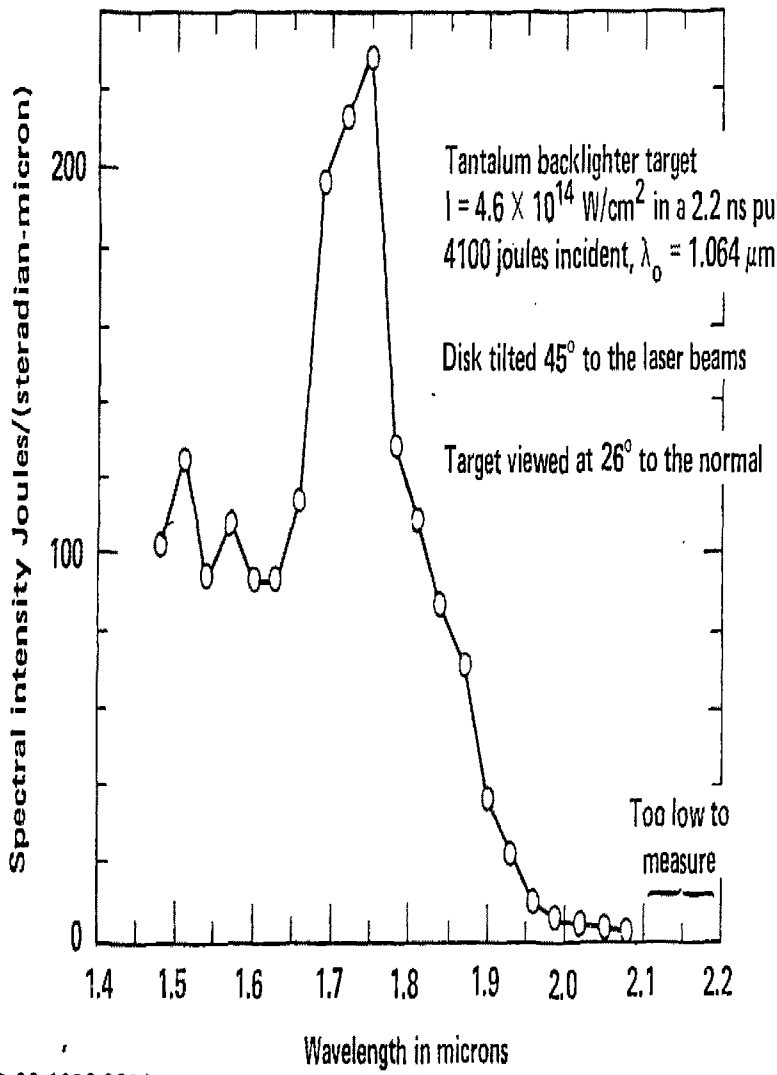

20-90-1080-3332

Figure 7

DECONVOLVED SIGNAL FROM A FAST PYRO-ELECTRIC DETECTOR SHOWS RAMAN LIGHT MOST INTENSE LATE IN THE LASER PULSE

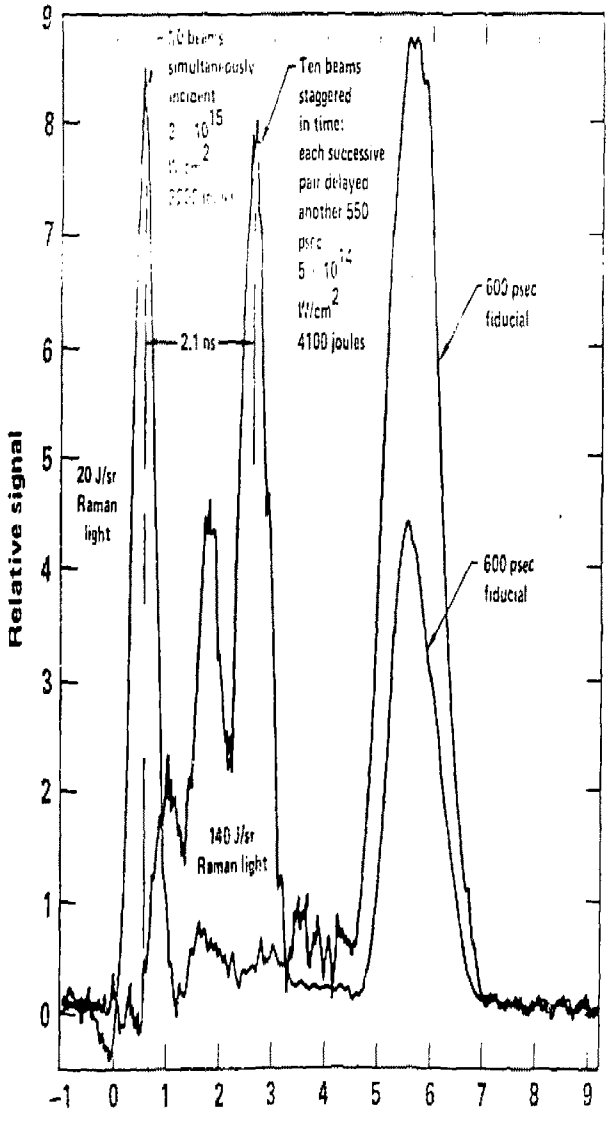

20-90-1080-3515

Figure 8

CALCULATED LASER POWER ON TARGET FOR 5×10^{14} W/cm^2, 2.2 ns TANTALUM DISK EXPERIMENT

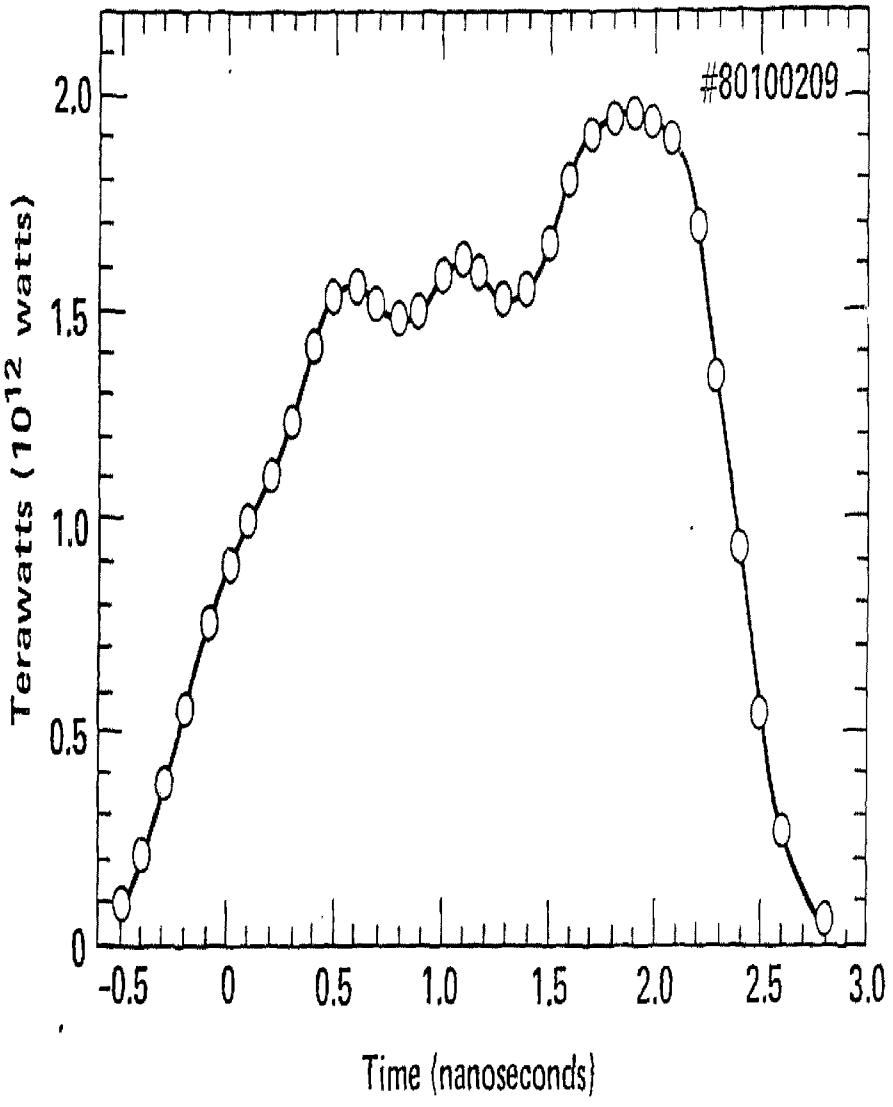

20-90-1080-3817

SPECTRUM OF THE RAMAN-SCATTERED LIGHT – 5 X 10^{14} W/cm^2, 800J, INS

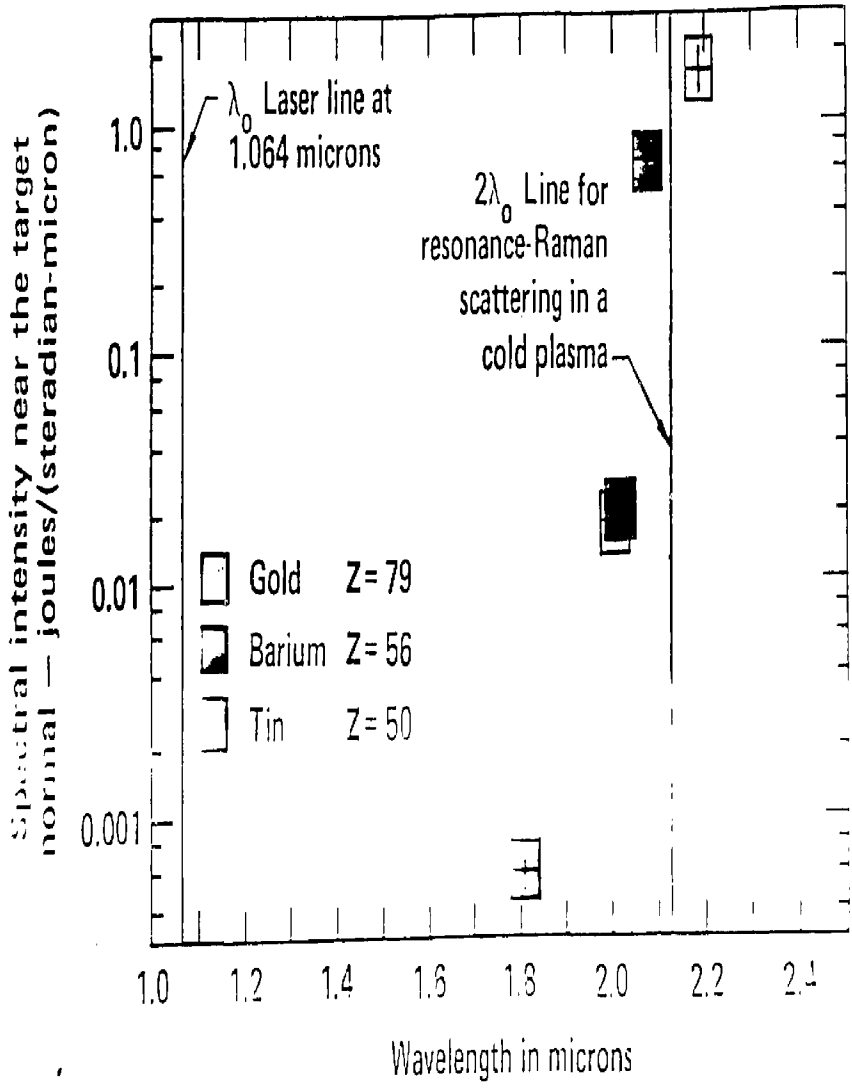

20-01-0380-0959

Figure 10

THE WAVE-BREAKING ENERGY INCREASES WITH THE BACKGROUND ELECTRON TEMPERATURE

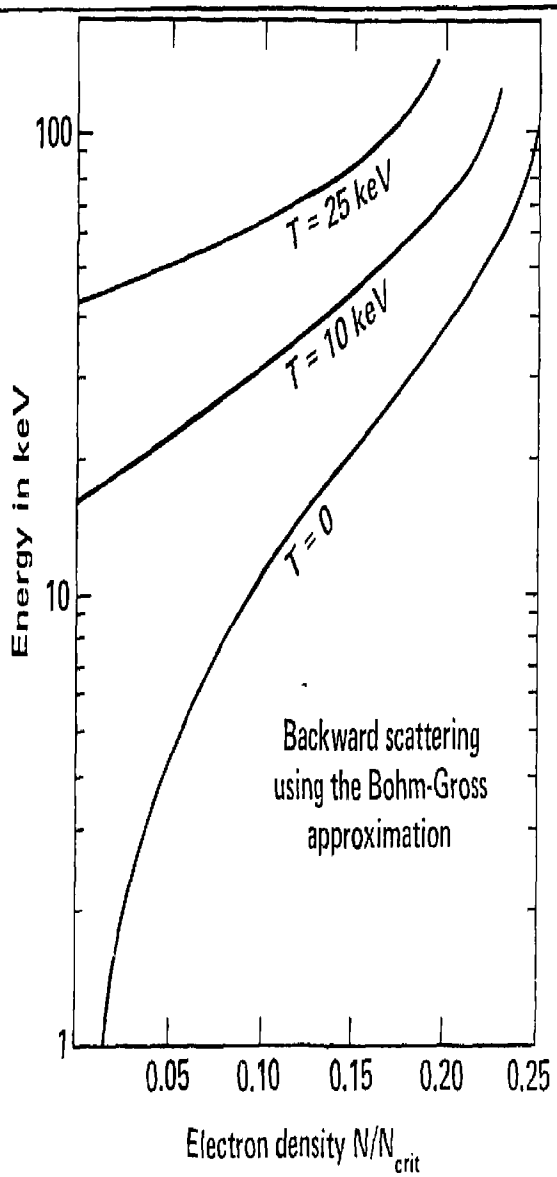

20-90-0879-2761

Figure 11

KINETIC ENERGY OF AN ELECTRON MOVING AT THE PHASE VELOCITY OF THE ELECTRON PLASMA WAVE PRODUCED BY THE RAMAN INSTABILITY IN A COLD PLASMA

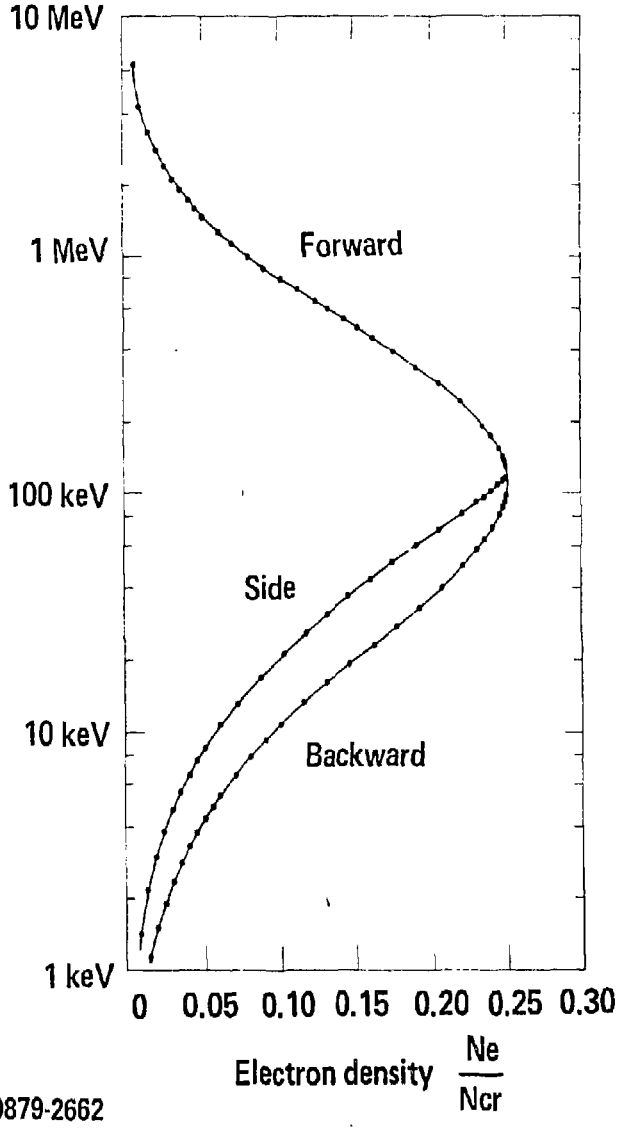

20-90-0879-2662

Figure 12

Raman light from Au microdiscs shows strong polarization dependence

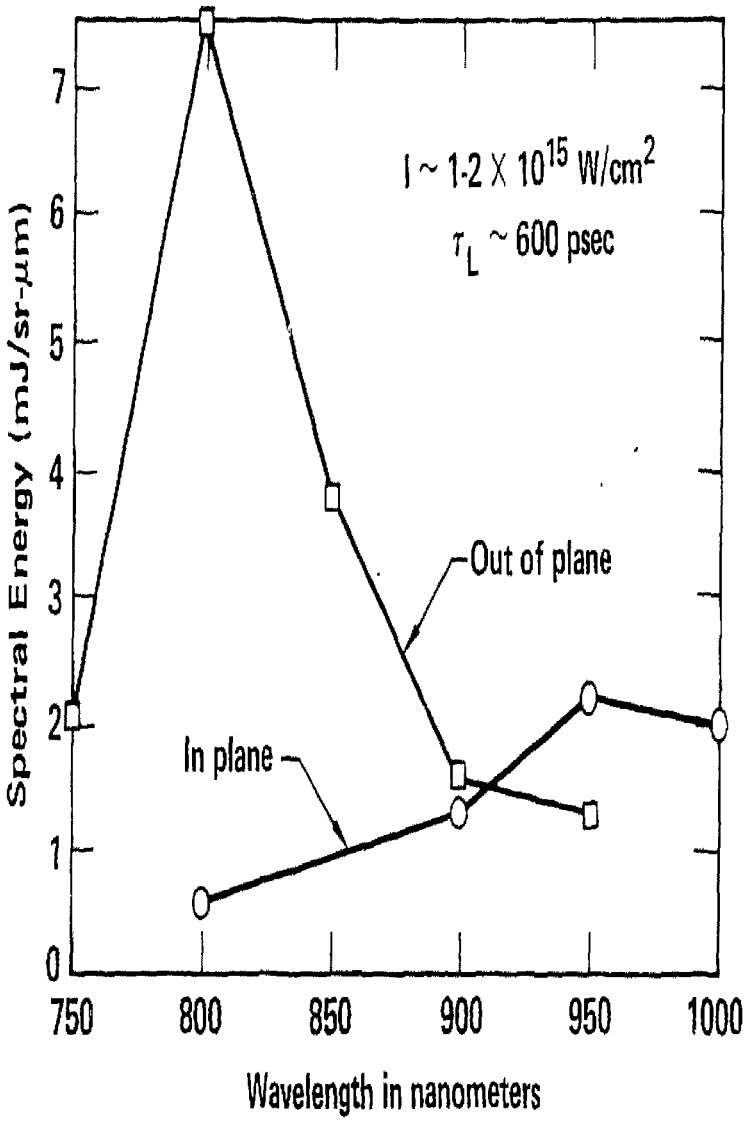

20-90-0980-2881

Figure 1s

COMPARISON OF THE SOLUTIONS TO THE DISPERSION EQUATIONS FOR SIDE AND BACK SCATTER AT 5 keV

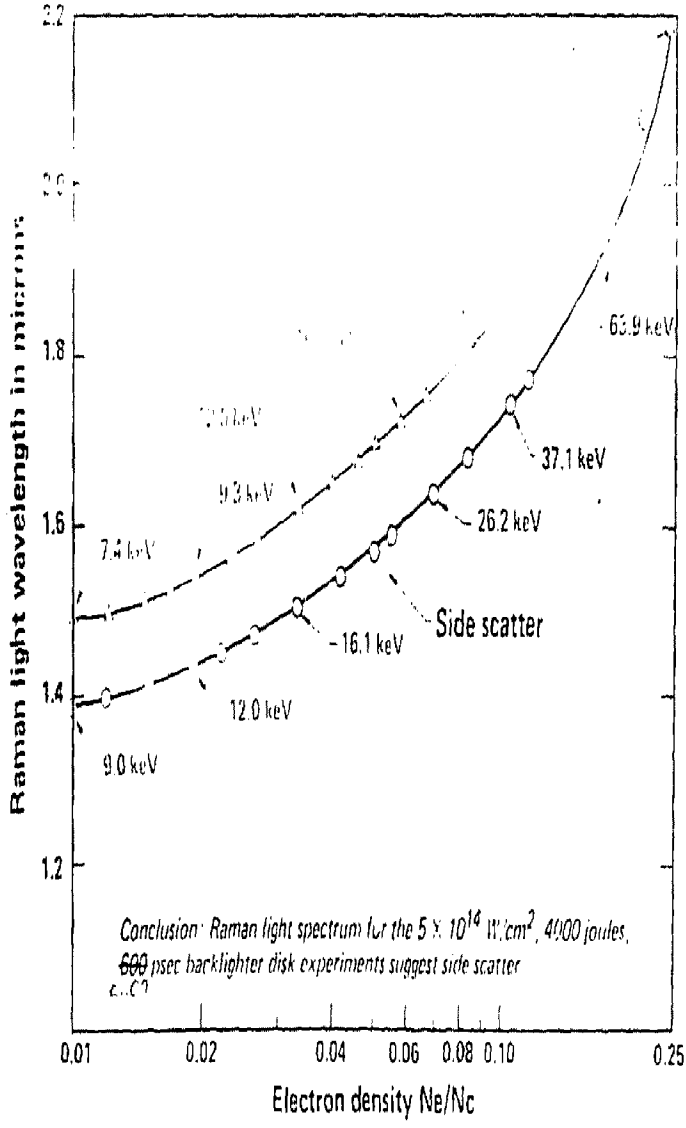

Figure 14

RAMAN LIGHT GENERATION IS OPTIMAL WHEN THE ELECTRON PLASMA WAVE IS DRIVEN NEARLY RESONANTLY AT THE TURNING DENSITY OF THE RAMAN-SHIFTED LIGHT WAVE

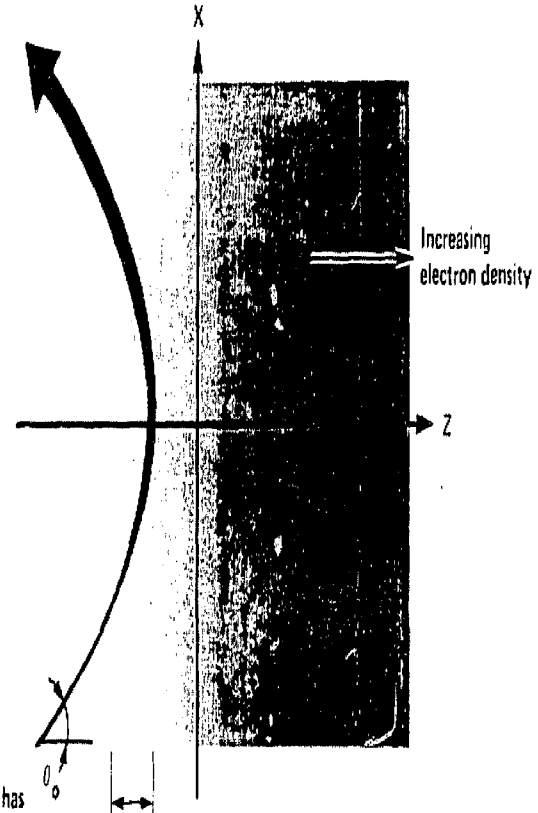

20-90-0979-2957

PYRO-ELECTRIC DETECTOR MEASUREMENTS OF THE RAMAN LIGHT ENERGY

Experiment description

Target	Energy	Pulse length	Intensity	Tilt Angle	Viewing Angle	Measured intensity
Ti disk	0.53 kJ	625 psec	3.6×10^{15} W/cm^2	45°	62°	2.4 J/SR
Hf disk	2.6 kJ	600 psec	4.6×10^{15} W/cm^2	45°	62°	67.4 J/SR
Ti disk	3.32 kJ	600 psec	2.0×10^{16} W/cm^2	45°	62°	4.2 J/SR
Ti disk	3.83 kJ	710 psec	3.5×10^{16} W/cm^2	45°	62°	4.2 J/SR
Zn disk	3.84 kJ	659 psec	$\sim 10^{17}$ W/cm^2	45°	62°	3.6 J/SR
HEET disk	2.97 kJ	600 psec	3×10^{15} W/cm^2	0°	20°	6.0 J/SR
HEET disk	3.19 kJ	600 psec	3.2×10^{15} W/cm^2	0°	20°	17.5 J/SR
HEET disk	3.29 kJ	600 psec	3.3×10^{15} W/cm^2	0°	20°	17.5 J/SR
HEET disk	1.77 kJ	600 psec	1.8×10^{15} W/cm^2	0°	20°	1.4 J/SR

Measurements made by Dave Banner, Lawrence Livermore laboratory

20-90-1080-3258

RAMAN LIGHT MEASUREMENTS FOR GOLD DISKS IRRADIATED AT HIGH INTENSITY

Experiment description	Spectral intensity measurements			
	1.6 μm	1.8 μm	2.0 μm	2.13 μm
$\sim 10^{16}$ W/cm^2				
100 μm diam spot 600 joules in 600 psec Target tilted 30° toward the light collector	0.33 joules/ (SR-μm) IN PLANE $\Delta\theta = 5.6°$	> 0.26 joules/ (SR-μm) IN PLANE $\Delta\theta = 7.2°$	—	0.4 – 1.1 joules/ (SR-μm) IN PLANE $\Delta\theta = 11.2°$
$\sim 10^{17}$ w/cm^2				
Best focus spot 900 joules in 1000 psec Targets irradiated at normal incidence	1.3 – 1.7 joules/ (SR-μm) IN PLANE $\Delta\theta = 25°$	0.84 joules/ (SR-μm) IN PLANE $\Delta\theta = 25°$	1.2 joules/ (SR-μm) IN PLANE $\Delta\theta = 25°$	—